NUREG/CR-3910
BNL-NUREG-51806

DYNAMIC SIMULATION OF THE AIR-COOLED DECAY HEAT REMOVAL SYSTEM OF THE GERMAN KNK-II EXPERIMENTAL BREEDER REACTOR

Bernd K. Schubert

Date Published — July 1984

CODE DEVELOPMENT, VALIDATION AND APPLICATION GROUP
DEPARTMENT OF NUCLEAR ENERGY, BROOKHAVEN NATIONAL LABORATORY
UPTON, NEW YORK 11973

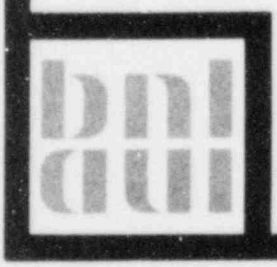

Prepared for the U.S. Nuclear Regulatory Commission
Office of Nuclear Regulatory Research
Contract No. DE-AC02-76CH00016

NUREG/CR-3910
BNL-NUREG-51806
AN

DYNAMIC SIMULATION OF THE AIR-COOLED DECAY HEAT REMOVAL SYSTEM OF THE GERMAN KNK-II EXPERIMENTAL BREEDER REACTOR

Bernd K. Schubert*

---

*Visiting scientist from GKSS-Forschungszentrum Geesthacht Germany

Manuscript Completed — June 1984
Date Published — July 1984

CODE DEVELOPMENT, VALIDATION AND APPLICATION GROUP
DEPARTMENT OF NUCLEAR ENERGY
BROOKHAVEN NATIONAL LABORATORY
ASSOCIATED UNIVERSITIES, INC.
UPTON, LONG ISLAND, NEW YORK 11973

CONTRACT NO. DE-AC02-76CH00016
FIN NO. A-3015

NOTICE

Available from
GPO Sales Program
Division of Technical Information and Document Control
U.S. Nuclear Regulatory Commission
Washington, D.C. 20555
and
National Technical Information Service
Springfield, Virginia 22161

ABSTRACT

A Dump Heat Exchanger and associated feedback control system models for decay heat removal in the German KNK-II experimental fast breeder reactor are presented. The purpose of the controller is to minimize temperature variations in the circuits and, hence, to prevent thermal shocks in the structures. The basic models for the DHX include the sodium-air thermodynamics and hydraulics, as well as a control system. Valve control models for the primary and intermediate sodium flow regulation during post shutdown conditions are also presented. These models have been interfaced with the SSC-L code. Typical results of sample transients are discussed. This type of study points up the versatility in the usage of SSC. SSC is a user-oriented, modular computer code that is developed in a very generic fashion. The interfacing of these KNK-II plant-specific models into SSC was accomplished in a straightforward and relatively easy manner.

TABLE OF CONTENTS

NOMENCLATURE

t	Time
T	Temperature
c_p	Spec. Heat Capacity
P	Pressure
m	Mass
W	Flow
q	Heat Transfer Rate
F_{COR}	Correction Factor
h	Heat Transfer Coefficient
A	Area
Nu	Nu-Number
Re	Re-Number
L	Length
K	Pressure Loss Coefficient
C	Drag Coefficient
n_t	Number of Tubes
D_h	Hydraulic Diameter
f	Friction Factor
H	Fan Head
g	Gravitational Constant
M	Torque
N	Speed
I	Inertia
a_{DAMP}	Constant
X	Variables
G	Gain Factor
P	Proportional Rate
R	Repetition Rate
Tr	Trim Signal
V	Volume
H	Valve Position (in 3.1)
F_o	Valve Speed
I_{TR}	Driver Flag
P	Power (in 3.1)
q	Volume Flow Rate (in 3.1)
Δz	Chimney Height or Elevation Difference

GREEK SYMBOLS

ζ	Density
α	Flap Open/Close Ratio
ϵ	Error
τ	Time Constant

SUBSCRIPTS

a	Actual
AIR	Air
Ang	Blade Angle
D	Demand
DAMP	Flaps
Fan	Fan
Fri	Friction
HT	Heat Exchanger
Hyd	Hydraulic
IN	In
k	Chimney
log	Logarithm
m	Measured
Mot	Motor
NA	Sodium
OUT	Out
P	Plenum
p	Pipe
Ref	Reference Value
Tr	Trim

LIST OF FIGURES

LIST OF FIGURES

LIST OF TABLES

ACKNOWLEDGEMENT

The author wishes to thank the SSC Code Development, Validation and Application Group for their help and support of this work and the arrangement of the author's stay at Brookhaven National Laboratory. In particular, he wishes to thank M. Khatib-Rahbar for valuable discussions; R.J. Kennett, who helped in computer specific questions and in interfacing with SSC, as well as Carmen Falkenbach for typing this report.

1. INTRODUCTION

As part of its work for LMFBR safety analysis the GKSS-Forschungszentrum Geesthacht plans the calculation of natural circulation transients of the German reactor KNK-II [1] with the system code SSC [2]. Special features of this reactor system include: 1) a Dump Heat Exchanger (DHX) in the secondary loop, which removes the decay heat after reactor scram and 2) control valves in both primary and secondary loops, which control the sodium flow rates under natural circulation conditions to keep loop temperatures constant and to prevent the structures against thermal shocks. These features are also being discussed or partly used for other reactors, such as the SNR-300 or Superphenix II. Figure 1.1 shows schematically the KNK-II reactor plant. If scram occurs, all pumps are tripped and the DHX flaps open. At the same time, controllers and their associated control valves are activated. The steam generator is bypassed on the sodium side. The DHX sodium outlet temperature is controlled to a constant pre-scram value by adjusting the air flow rate [3]. Because the present SSC version cannot simulate these KNK-II plant specific DHX and associated controls, models have been separately developed and are presented in this report.

2. HEAT EXCHANGER MODEL

The heat exchanger configuration used in the model is shown in Figure 2.1. The heat exchanger is of the single pass, cross-flow design using finned tubes. Heat can be removed by either natural or forced convection. Since the sodium outlet temperature has to remain approximately constant, the air flow rate is controlled: 1) by flaps and/or adjustable blade angle, keeping the fan speed constant or 2) by variable fan speed, keeping the blade angle constant.

For the modeling of the heat exchanger and the hydraulic response, the following assumptions apply:

- one dimensional flow
- no axial heat conduction

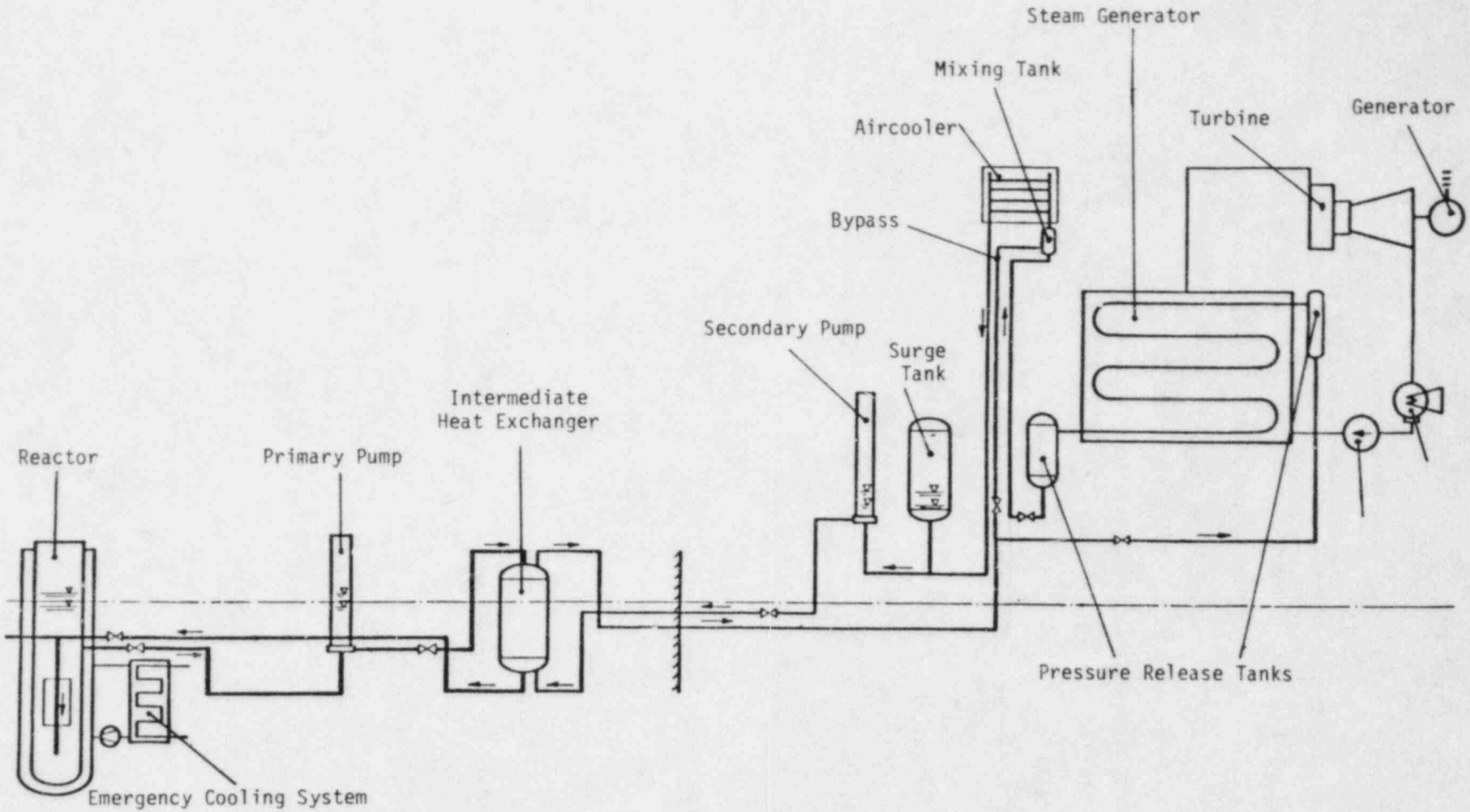

Figure 1.1 KNK-II Plant Layout

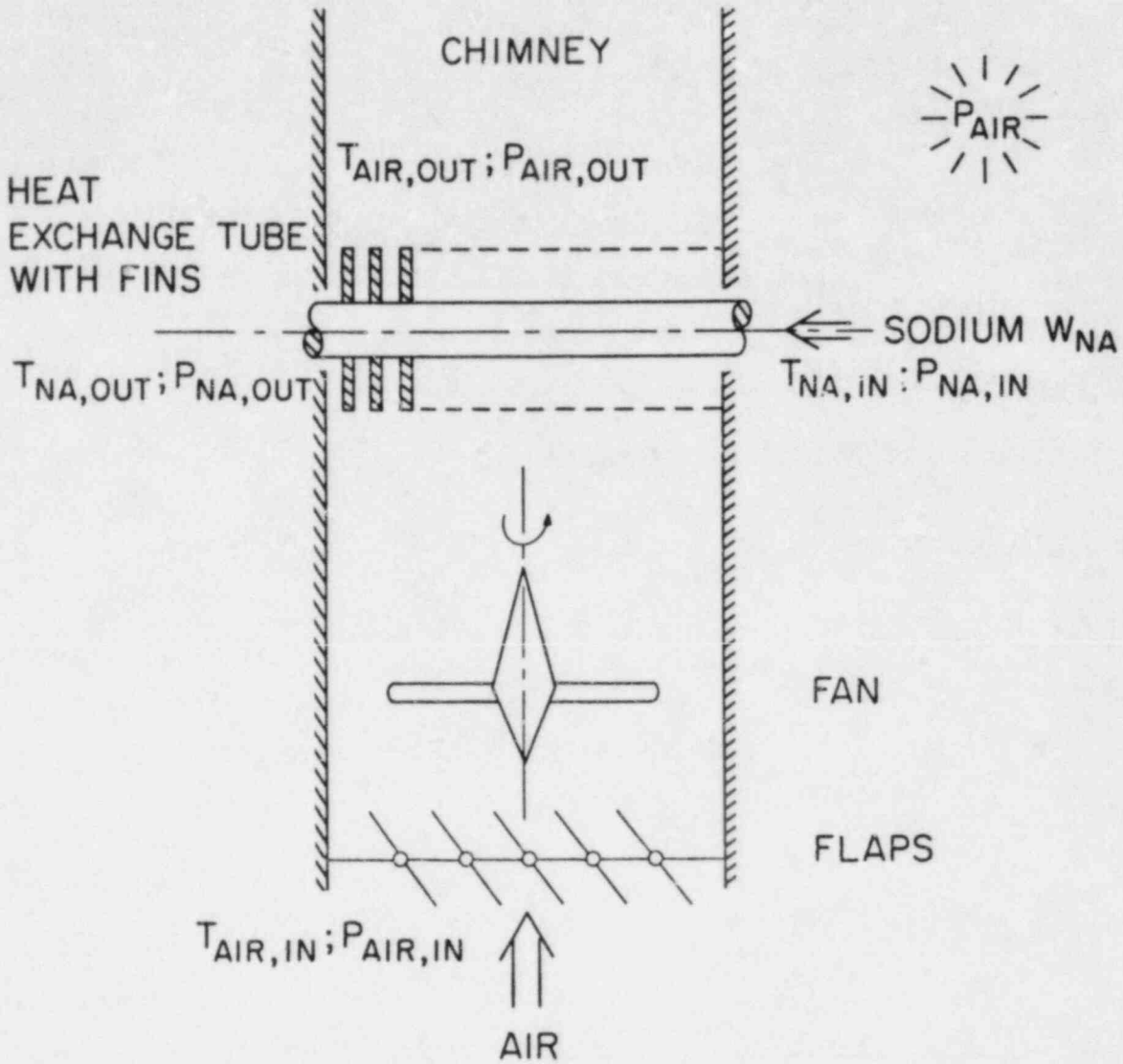

Figure 2.1 Dump Heat Exchanger Model Arrangement

- incompressible fluids
- the logarithmic mean temperature is valid
- the heat transfer mechanism of the air-side dominates the whole heat transfer process
- air is treated as ideal gas, i.e.,

$$\rho \sim \frac{1}{T} \tag{1}$$

- thermal and hydraulic inertias of air are neglected, i.e.,

$$\frac{dW}{dt} = 0, \quad \frac{dT}{dt} = 0 \tag{2}$$

2.1 THERMAL MODEL

The energy equation for the DHX sodium side is written as:

$$(c_p m)_{NA} \frac{dT_{NA}}{dt} = W_{NA} (c_{p_{NA,IN}} T_{NA,IN} - c_{p_{NA,OUT}} T_{NA,OUT}) - q \tag{3}$$

and for the air side as:

$$W_{AIR} (c_{p_{AIR,IN}} T_{AIR,IN} - c_{p_{AIR,OUT}} T_{AIR,OUT}) + q = 0 \tag{4}$$

q is defined as

$$q = F_{COR} \; h \; A_{HT} \; \Delta T_{log} \tag{5}$$

where

$$\Delta T_{log} = \frac{(T_{NA,IN} - T_{AIR,OUT}) - (T_{NA,OUT} - T_{AIR,IN})}{\ell n \left(\frac{T_{NA,IN} - T_{AIR,OUT}}{T_{NA,OUT} - T_{AIR,IN}}\right)} \tag{6}$$

The use of the log mean temperature difference approach is exactly valid only in the case of counter-current flow. The application to a cross-flow heat exchanger is done by introducing a correction factor F_{COR} considering the reduced heat transfer rate under these conditions. The factor can be obtained from diagrams given by various authors, e.g., [4].

The air-side Nusselt number is given by Briggs and Young [5]

$$Nu = 0.134\, Re^{0.681}\, Pr^{0.333} \left(\frac{s}{L}\right)^{0.2} \left(\frac{s}{t}\right)^{0.1134} \tag{7}$$

where s is the distance between adjacent fins, t is the fin thickness and L is the fin height.

2.2 HYDRAULIC MODEL

In order to utilize the SSC integrator package, the momentum equation is written as follows, where for air, the left hand side is neglected and the air flow is explicitly calculated from the resulting equation:

$$\Sigma \frac{L}{A} \frac{dW}{dt} = P_{IN} - P_{OUT} - \Sigma \Delta P \tag{8}$$

The pressure drop term in Equation (8) for sodium is:

$$\Sigma \Delta P_{NA} = \frac{W_{NA}^2}{A_P^2}\left(\frac{1}{\rho_{NA,OUT}} - \frac{1}{\rho_{NA,OUT}}\right) + \frac{1}{2} \frac{W_{NA}|W_{NA}|}{D_{h,NA} A_P^2} \frac{f \cdot L}{\bar{\rho}}$$

$$+ K_{IN} \frac{W_{NA}|W_{NA}|}{\rho_{NA,IN} A_{IN}^2} + K_{OUT} \frac{W_{NA}|W_{NA}|}{\rho_{NA,OUT} A_{OUT}^2} + K_{P_{IN}} \frac{W_{NA}|W_{NA}|}{\rho_{NA,IN} A_P^2}$$

$$+ K_{P_{OUT}} \frac{W_{NA}|W_{NA}|}{\rho_{NA,OUT} A_P^2} + g\Delta Z \left(\rho_{NA,OUT} - \rho_{NA,IN}\right) \tag{9}$$

where

$$A_P = n_t \frac{\pi D_{h,NA}^2}{4} \tag{10}$$

$f = f(Re, \varepsilon)$ obtained from [2]

For air:

$$\Sigma\Delta P_{NA} = \frac{W_{AIR}^2}{A_K^2}\left(\frac{1}{\rho_{AIR,OUT}} - \frac{1}{\rho_{AIR,IN}}\right) + K_{K,IN}\frac{W_{AIR}^2}{\rho_{AIR,IN}\,A_K^2}$$

$$+ K_{K,OUT}\frac{W_{AIR}^2}{\rho_{AIR,OUT}\,A_K^2} + f_{HT}\frac{W_{AIR}^2}{\bar{\rho}_{AIR}\,A_{Hyd}^2} + f_{DAMP}\frac{W_{AIR}^2}{\rho_{AIR,IN}\,A_K^2}$$

$$+ g\Delta Z\left(\frac{1}{\rho_{AIR,OUT}} - \frac{1}{\rho_{AIR,IN}}\right) - \Delta P_{Fan} = 0 \qquad (11)$$

$$\bar{\rho}_{AIR} = \frac{1}{2}\left(\rho_{AIR,IN} + \rho_{AIR,OUT}\right) \qquad (12)$$

$$f_{HT} = \Delta P_{HT,Ref}\,\frac{\rho_{AIR,Ref}\,A_{Hyd}^2}{W_{AIR,Ref}^2} \qquad (13)$$

2.3 FAN MODEL

In order to simulate the fan behavior under accident conditions (e.g., station blackout) or air flow control with variable fan speed instead of variable blade angle, polynomial expressions for the fan operating characteristic curves are derived as described by the homologeous theory [6]. The polynomial coefficients are based on values given by Cady [7]. These values were obtained from FFTF measurements (see Table 2.1). They do not necessarily fit those measured in KNK-II, but because of the lack of sufficient KNK-II data and because the general behavior of fans should not be much different, these values are used in the present model. In addition, the adjustable fan blade angle is modeled by a given function multiplied with polynomial results.

$$\Delta P_{FAN} = \rho_{AIR,IN} \cdot g \cdot H_{Ref} \cdot \sin\left(\frac{\pi}{2} \cdot \theta\right) \begin{cases} \Omega^2 \sum_{1}^{5} a_i \left(\frac{\nu}{\Omega}\right)^{i-1} & ; \quad \nu \leq \Omega \\ \nu^2 \sum_{1}^{5} b_i \left(\frac{\Omega}{\nu}\right)^{i-1} & ; \quad \nu > \Omega \end{cases} \tag{14}$$

$$M_{Hyd} = \sin\left(\frac{\pi}{2} \cdot \theta\right) \begin{cases} \Omega^2 \sum_{1}^{5} c_i \left(\frac{\nu}{\Omega}\right)^{i-1} & ; \quad \nu \leq \Omega \\ \nu^2 \sum_{1}^{5} d_i \left(\frac{\nu}{\Omega}\right)^{i-1} & ; \quad \nu > \Omega \end{cases} \tag{15}$$

where $\Omega = \frac{N}{N_{Ref}}$, $\nu = \frac{W}{W_{Ref}}$, $M_{Hyd} = \frac{M}{M_{Ref}}$ and $\theta = \frac{\theta_{actual}}{\theta_{max}}$

Table 2.1 Polynomials Coefficients for Fan Performance Curves

a_i	b_i	c_i	d_i
1.17	3.4	0.31	-1.0
0.24	3.0	0.85	2.6
0.0	3.9	0.0	-0.35
-0.1	-2.5	-0.04	0.35
-0.31	0.0	-0.12	0.0

The dynamic behavior of the fan is given by an angular momentum equation

$$\tau_{Fan} \frac{d\Omega}{dt} = M_{Mot} - M_{Hyd} - M_{Fri} \tag{16}$$

This equation uses normalized values. Therefore, τ_{Fan} becomes

$$\tau_{Fan} = \frac{I \cdot N \cdot 2\pi}{60 \cdot M_{Ref}} \tag{17}$$

The momentum loss due to friction is modeled by the following relations as proposed by Cady [7]. Because the momentum loss due to friction only becomes important under low pump speed conditions, the equation is limited to low pump speeds.

$$M_{Fri} = \begin{cases} 0.04 \left(1 - \frac{\Omega}{0.065}\right), & \Omega \leq 0.065 \\ 0 \quad , & \Omega > 0.065 \end{cases} \tag{18}$$

For the motor torque it is assumed that the pump shaft and the impeller are accelerated until they reach design speed at the full design torque. After pump trip, the pump torque becomes zero.

$$M_{Mot} = \begin{cases} 1. & \Omega < 1. \\ M_{Hyd} & \Omega = 1. \\ 0. & \text{after pump trip} \end{cases} \tag{19}$$

During normal operation, the air cooler chimney is closed by flaps which cause the heat exchanger pipes to remain in an almost adiabatic condition, as assumed in the previously described model. However, after scram occurs, these flaps open automatically and air circulates through the chimney. It has been found that during air cooler start-up transients, air flow caused only by natural convection can become high enough to drop the sodium outlet temperature substantially below the setpoint. To avoid such behavior, the flaps are incorporated in the control process and act as a control device via the pressure drop, as well as the adjustable fan blade. The governing equations for the flaps are:

$$\Delta P_{DAMP} = f_{DAMP} \frac{W_{AIR}^2}{A_K^2 \rho_{AIR,IN}} \tag{20}$$

where

$$f_{DAMP} = \begin{cases} 10^{10} & ; \quad \alpha = 0 \\ \dfrac{f_{DAMP,0}}{\alpha_{DAMP}^2} & ; \quad 0 < \alpha \leq 1.0 \end{cases} \tag{21}$$

and $f_{DAMP,0}$ is the pressure drop coefficient for flaps at their fully open position. For this case, $f_{DAMP,0}$ is chosen at 0.25.

2.4 CONTROLLER MODEL

A controller is used to adjust the air cooler sodium outlet temperature to its pre-scram value. Figure 2.2 shows the principal arrangement. The controller chain consists of two cascades, where the second cascade uses a proportional-integral-differential controller. Controlled variables are the air cooler sodium inlet and outlet temperatures. To obtain better control behavior, the error signal of the inlet temperature is added via a differential controller to the main controller inlet. The assigned temperatures before scram serve as setpoint values. The models used to describe the controlling chain are those suggested by Khatib-Rahbar [8] and explained in more detail therein. A block diagram of a unit controller is shown in Figure 2.3. The governing equations are as follows:

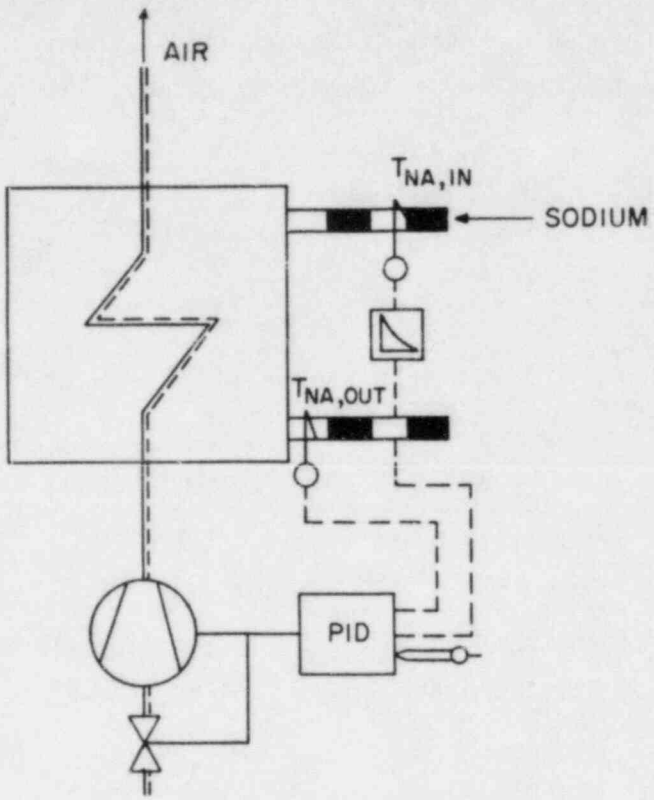

Figure 2.2 Principal Controller Arrangement

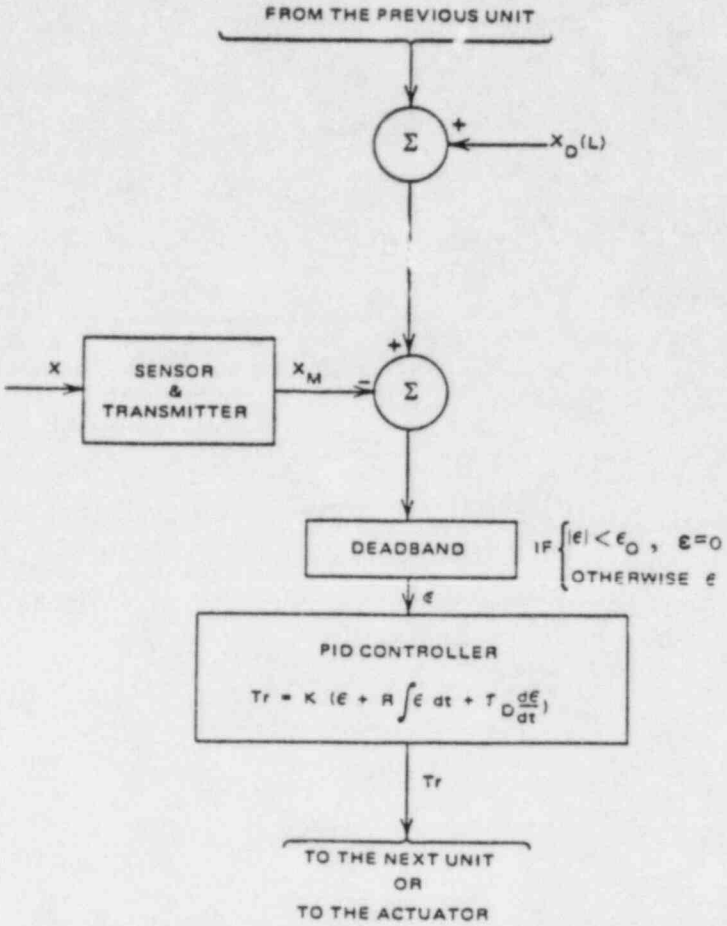

Figure 2.3 Block Diagram Representation of the Unit Controller

- Comparator

$$\varepsilon = X_D + X_{Tr} - X_m \tag{22}$$

- Sensor

$$\tau_m \frac{dX_m}{dt} = X_a - X_m \tag{23}$$

- Deadband

$$\begin{aligned} |\varepsilon| &> \varepsilon_o \Longrightarrow \varepsilon = \varepsilon \\ |\varepsilon| &\leq \varepsilon_o \Longrightarrow \varepsilon = 0 \end{aligned} \tag{24}$$

- P D - Controller

$$Tr = G(P\varepsilon + R \int_{t=0}^{t} \varepsilon dt + \tau_D \frac{d\varepsilon}{dt}) \tag{25}$$

where the integral and the derivative terms are numerically approximated by:

$$\int_{t=0}^{t} \varepsilon dt \approx \sum_{k=1}^{n} (\varepsilon^k \Delta t) \qquad \text{and} \tag{26}$$

$$\frac{d\varepsilon}{dt} \approx \frac{\varepsilon^k - \varepsilon^{k-1}}{dt} \tag{27}$$

The dynamics of the power element flaps and fan blades are described by first order differential equations with higher order influences neglected. That is:

- Variable Blade Angle

$$\tau_{Ang} \frac{d\theta}{dt} = \theta_D - \theta \tag{28}$$

where $\theta_D = \theta_o + Tr$.

Variable Flaps

$$\tau_{DAMP} \frac{d\alpha}{dt} = \alpha_D - \alpha \tag{29}$$

where $\alpha_D = \alpha_o + Tr.$

2.5 NUMERICAL CONSIDERATIONS

The assumption that both fluids can be treated as incompressible, simplifies the numerical solution significantly. Because the hydraulic equations depend only slightly on the energy equations, whereas on the other hand the temperature field is strongly coupled to the flow rate, the hydraulics is solved first, using the temperatures of the last time step. The energy equation is then solved utilizing the updated flow rate. This method influences the code structure as shown in Figure 2.4. A more detailed description of the subroutines is given in Appendix A.

The sodium energy equation is transformed into a finite-difference equation for the numerical solution. Assuming that:

$$\frac{d\bar{T}_{NA}}{dt} \approx \frac{dT_{NA,OUT}}{dt} \quad , \tag{30}$$

leads to (see Figure 2.5):

$$c_p(\bar{T})\ \rho(\bar{T})\ V \frac{T^{K+1}_{NA,I+1} - T^{K}_{NA,I+1}}{\Delta t} = c_p\ (T^{K+1}_{i}) \cdot W_{NA}\ T^{K+1}_{NA,i} - c_p\ (T^{K}_{NA,i+1}) \cdot W_{NA} T^{K+1}_{NA,i+1} - q \tag{31}$$

or

$$T^{K+1}_{NA,i+1} = \frac{c_p(\bar{T})\ \rho(\bar{T})\ V \frac{T^{K}_{NA,i+1}}{\Delta t} + c_p(T^{K+1}_{i}) \cdot W_{NA}\ T^{K+1}_{NA,i} - q}{C} \tag{32}$$

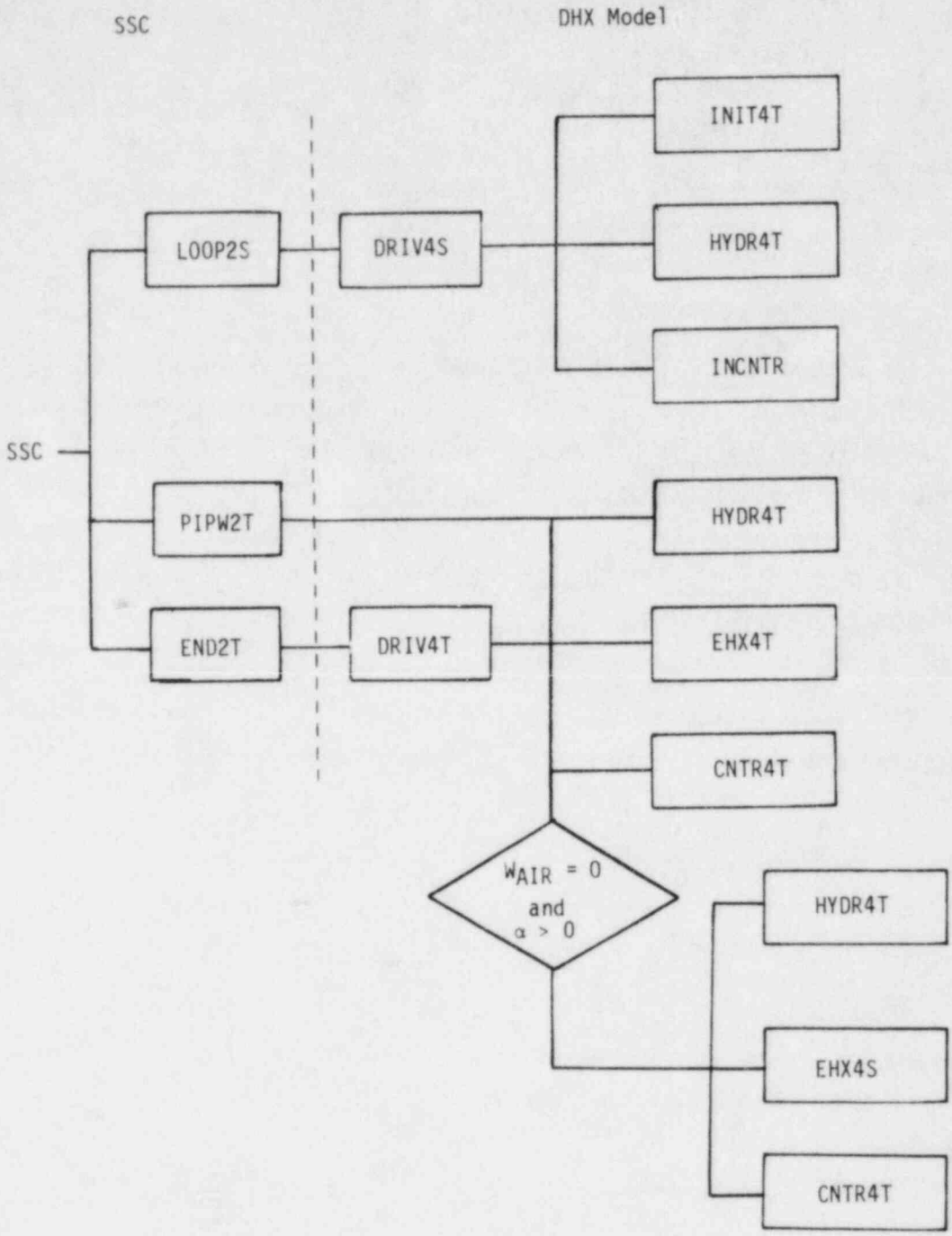

Figure 2.4 SSC-DHX Interconnection

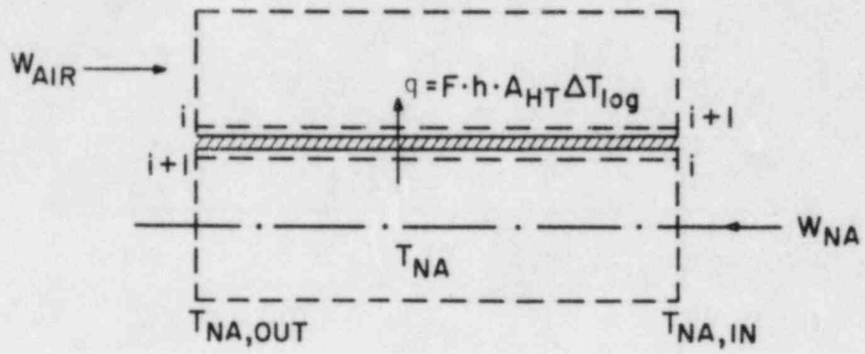

Figure 2.5 Control Volume for Energy Equation

where

$$C = c_p(\bar{T})\ \rho(\bar{T})\ \frac{V}{\Delta t} + c_p\ (T^k_{i+1})\ W_{NA} \tag{33}$$

$$V = \pi\ D_i^2\ \frac{\Delta X}{4} \tag{34}$$

$$\bar{T} = \frac{T_i^{k+1} + T_{i-1}^k}{2} \tag{35}$$

$$q = F_{COR}\ A_{HR}\ h(Re_{AIR}, Pr_{AIR})\ \Delta T_{log}/N \tag{36}$$

$$\Delta T_{log} = \frac{(T^k_{NA,i} - T^k_{AIR,i+1}) - (T^k_{NA,i+1} - T^k_{AIR,i})}{\ell n \left(\frac{T^k_{NA,i} - T^k_{AIR,i+1}}{T^k_{NA,i+1} - T^k_{AIR,i}} \right)} \tag{37}$$

For further numerical simplification, the source term uses the temperatures of the previous time step. The assumption made here is that the source term should vary only slightly during a transient, which is certainly the case in slow decay heat removal transients.

Because of the non-linearity of the source term and the small amount of mass on the air side (causing a small heat capacity), the air side energy equation is highly unstable when solved directly. Hence, this equation is solved iteratively for each time step with a Newton-Raphson procedure.

$$T^{k+1}_{AIR,i+1} = T^{k+1}_{AIR,i+1} - \frac{F(T^{k+1}_{AIR,i+n})}{F'(T^{k+1}_{AIR,i+1})} \tag{38}$$

$$F(T^{K+1}_{AIR,i+1}) = c_p\,(T^{K+1}_{AIR,i+1})\,W_{AIR}\,T^{K+1}_{AIR,i+1} - c_p\,(T^{K+1}_{AIR,i})\,W_{AIR}\,T^{K+1}_{AIR,i} - q \tag{39}$$

$$F'(T^{k+1}_{AIR,i+1}) = \frac{dF}{dT^{k+1}_{AIR,i+1}} \tag{40}$$

During operational transients, only the sodium equations must be solved and the source term (q) is equal to zero. At the beginning of a DHX start-up transient, q is indefinite for $W_{AIR} = 0$. Hence, a steady-state solution is first provided for the entire system where both energy equations are solved iteratively by Newton-Raphson.

The time derivative terms of the remaining equations given in the previous sections are all approximated by the same scheme of first order accuracy:

$$\frac{d\phi}{dt} \approx \frac{\phi^{k+1} - \phi^{k}}{\Delta t} \tag{41}$$

The air side hydraulic equation provides, explicitly, the air mass flow rate. However, for the sodium side hydraulics, the respective pressure terms are calculated and added to the overall secondary loop pressure loss, and the SSC integrator package calculates the advanced sodium flow rate.

In order to be sure that no numerical instabilities are caused by the sodium energy equation, several stability criteria, as given by Courant [9] and Madni [10], have been checked for different cases over their expected ranges. The results are depicted in Table 2.2. Comparing the most restrictive characteristic time constants with the SSC time steps calculated during test runs, it can be stated that these values are well within the range of values calculated by SSC. Therefore, an additional time step control for the model was not incorporated into the code.

Table 2.2 Comparison of Characteristic Time Constants
Using Different Criteria

$T_{NA} = 70C$ $\rho_{NA} = 850$ $c_{pN4} = 1270$	$\frac{\Delta X \cdot \rho \cdot A}{W_{NA}}$	$\frac{2m\ c_p}{h\ A_{AIR}}$	$\frac{m_{NA}\ c_p}{W_{NA}\ c_p + 0.5\ hA_{AIR}}$
$h = 0$ $W_{NA} = 125$	0.1	-	0.1
$h = 0$ $W_{NA} = 8.75$	1.5	-	1.5
$h = 4.5$ $W_{NA} = 8.75$	1.5	165	1.47
$h = 65.$ $W_{NA} = 8.75$	1.5	11.5	1.3
$h = 65.$ $W_{NA} = 25.$	0.52	11.5	0.5

T (K), ρ (Kg/m^3), c_p (J/(Kg · K)), h (W/(m^2 · K)),
W (Kg/s), x (m), m (Kg), A (m^2)

The interface between SSC and the DHX model is straightforward. SSC provides the DHX with sodium mass flow rate, the sodium inlet temperature and a scram flag, which indicates whether scram occurred or not for the DHX. The DHX itself delivers the sodium outlet temperature back to SSC.

3. POST SHUTDOWN CONTROL SYSTEM

During post scram conditions, the reactor power usually drops much faster than the core flow rate in the first few seconds. This results in a large and rapid temperature variation at the core outlet which may lead to thermal stress on the structures, thus eventually influencing the long term reliability of the plant. In order to reduce thermal stress, German plant designs use motor operated valves in the primary and intermediate loops to decrease and adjust the flow rate more rapidly to match the relative power and to minimize large temperature variations in the reactor circuits.

3.1 CONTROLLER CIRCUIT

The typical controller circuit for the flow control under natural circulation conditions is shown in Figure 3.1. The controlled variable is the flow rate in either the primary or secondary loop. This value is compared to the demanded flow rate which is a function of the produced power and, compared to the level before scram, the stored power in the system. A three point switch (on-off-on controller) uses the signal from the comparator to drive a valve motor.

The equations for comparator and sensor modeling are already given in Section 2.4. The three point switch model is shown in Figure 3.2. For the valve motion the following equation is used:

$$H^{k+1} = I_{Tr} \cdot \Delta t \cdot F_o + H^k \qquad (42)$$

Assuming that; 1) the specific heat capacity varies only slightly within the available, small temperature band (since it is determined by the part load behavior of the plant) and 2) the core temperature difference remains constant, the flow demand reduces to:

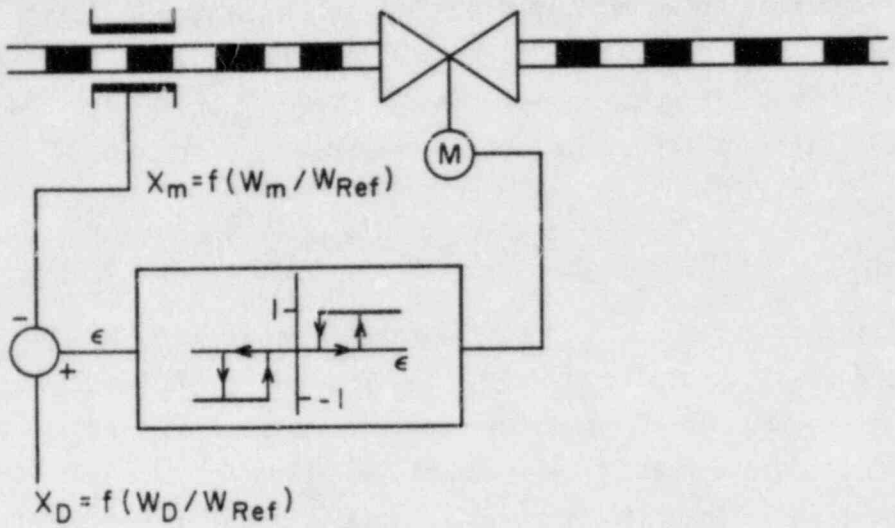

Figure 3.1 Controller Circuit for After Scram Flow Control

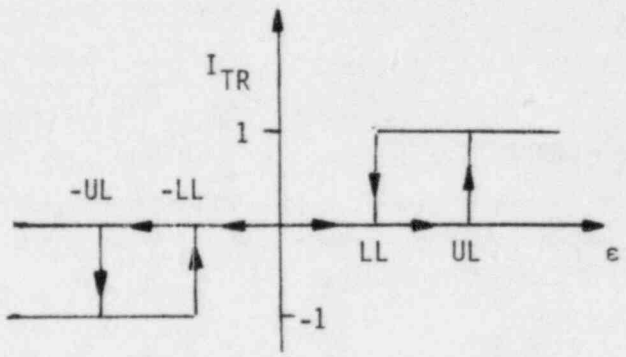

$$I_{TR}^{K+1} = \begin{cases} 1 & \epsilon \geq UL \\ & \epsilon \geq LL \wedge I_{TR}^{K} = 1 \\ 0 & |\epsilon| < LL \\ & |\epsilon| < UL \wedge I_{TR}^{K} = 0 \\ -1 & \epsilon \leq -UL \\ & \epsilon \leq -LL \wedge I_{TR}^{K} = 1 \end{cases}$$

Figure 3.2 Three-Point Switch Model

$$X_D = P/P_{Ref} \tag{43}$$

where the stored power is neglected in the present model.

The impact of the valve is felt through its pressure loss which can be obtained by:

$$q = C_v \sqrt{\frac{\Delta P \ \rho_{Ref}}{\Delta P_{Ref} \rho}} \tag{44}$$

as it is given in [11]. The valve position dependent pressure loss is introduced by the drag coefficient C_v, which is a function of the valve stem position. Because the function is highly dependent on the valve design, no function is given here, but values can be found in [11].

4. RESULTS

The models described in the previous Sections have been coded , de-bugged and interfaced into SSC. Before the actual interfacing, they were tested on a stand-alone basis in order to assess model features and limitations, as well as the controller settings (summarized in Tables 4.1 and 4.2). As a reference transient, a sodium inlet temperature ramp of 3 K/s has been used, with the sodium flow rate kept constant at 9.5 kg/s. These values are within the expected range of the KNK-II experiments and the SSC-DHX calculations. The results are presented in Figures 4.1 - 4.4.

In Figure 4.4, the behavior of the air flow controller actuator elements is shown. After reactor scram, the DHX fan is started at once, whereas the blade angle is still kept at zero. When the sodium temperatures exceed the controller deadband, the flaps open. The DHX air outlet temperature drops immediately (Figure 4.1), causing the sodium outlet temperature to fall under the controller setpoint temperature. Thus, the flaps stop opening and the air flow rate remains almost constant for several seconds (Figure 4.2). Then the flaps continue to open. After 25(s) the flap opening reaches 7.5% of full open and the blade angle adjustment provides additional support for the air flow delivery.

The movement of the blade angle was initiated on the basis of the flap position of 7.5% in order to satisfy the air flow demand signal in a reasonable time scale. The influence of the flap motion on the air flow rate becomes less important after exceeding a value of 30% open and, hence, the flaps are decoupled from the controller signal and open at a higher constant rate.

Figure 4.3 illustrates that the DHX inlet sodium temperature stabilizes at about 813^{o}K, which corresponds to a 240^{o}K desired ΔT across the heat exchanger. The system then starts to settle down to steady conditions as is indicated by the slow decrease of the air flow rate.

Table 4.1 Air Cooler Controller Settings

Variable	Equation	Units	Value	
			Cascade 1	Cascade 2
Sensor Time Constant (τ_m)	(23)	s	0.1	0.1
Deadband (ε_o)	(24)	-	0.0	0.005
Controller Gain (G)	(25)	-	1.0	1.0
Proportional Gain (P)	(25)	-	0.0	1.0
Integral Repetition (R)	(25)	s^{-1}	0.0	0.01
Derivative Time (τ_D)	(25)	s	1.0	0.0

Table 4.2 Power Element Actuator Time Constants

Variable	Equation	Units	Value
Damper Constant (τ_{DAMP})	(29)	s	2.0*
Fan Constant (τ_{FAN})	(16)	s	16.0
Blade Constant (τ_{ANG})	(28)	s	2.0

*τ_{DAMP} = 30.0 when flap ratio (α) > 0.3

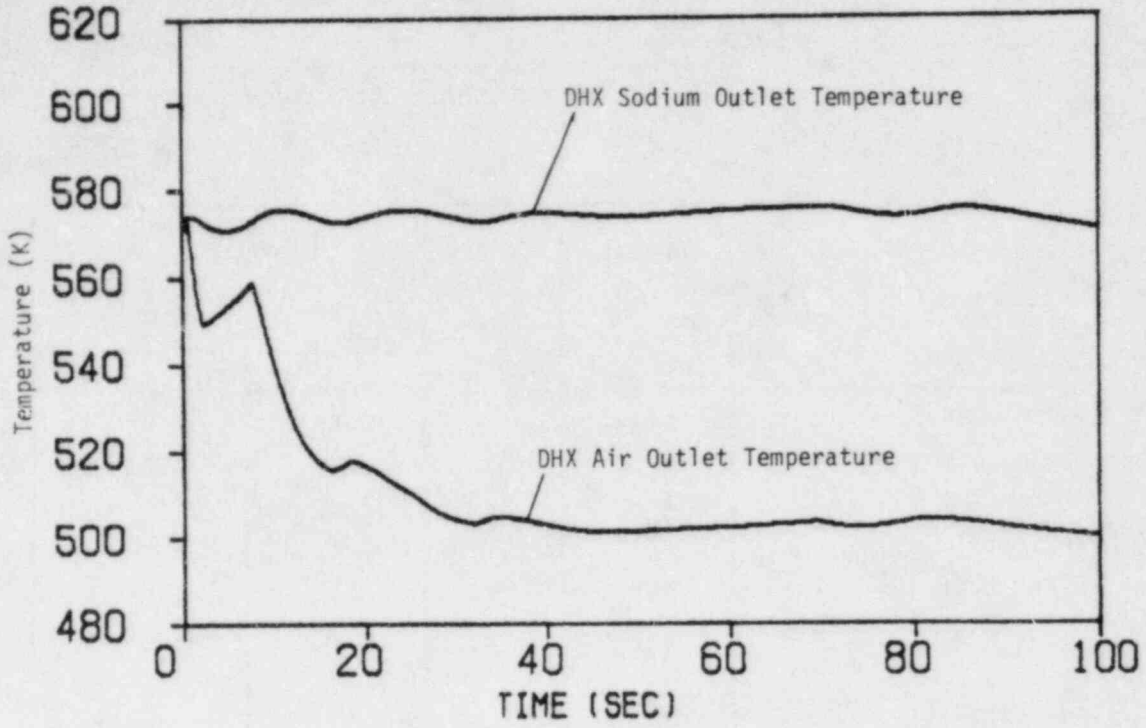

Figure 4.1 DHX - Outlet Temperatures (Ref. case)

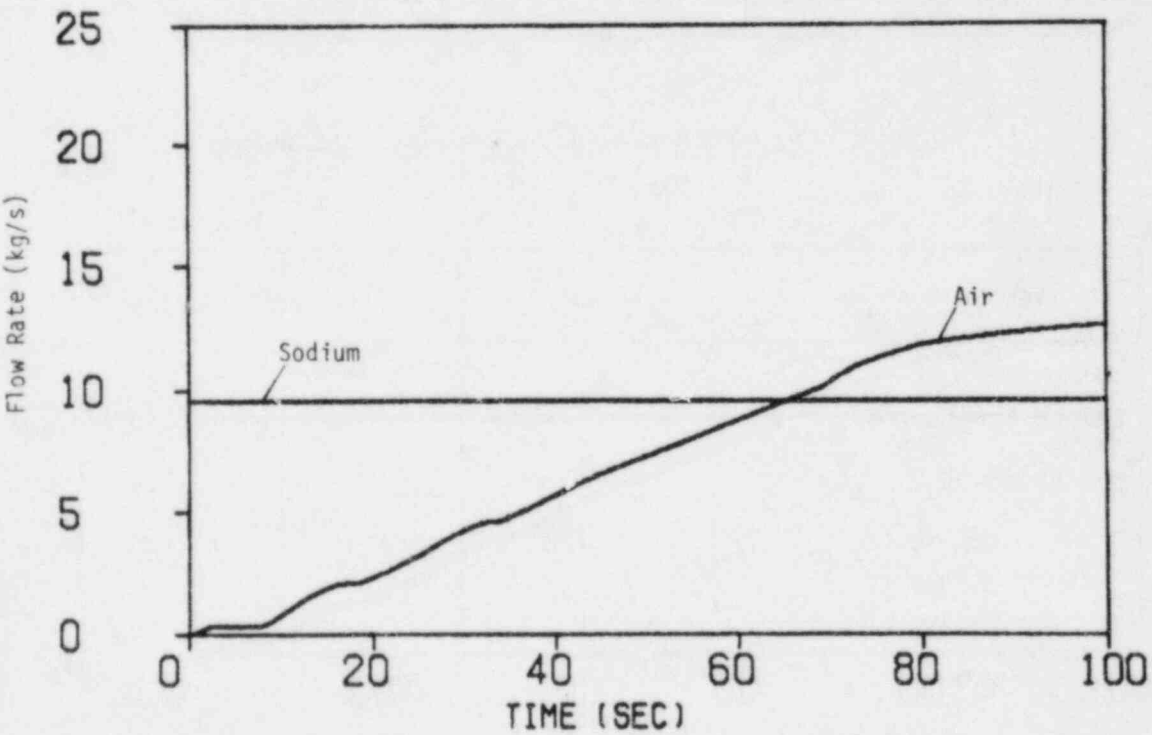

Figure 4.2 DHX - Flow Rates (Ref. case)

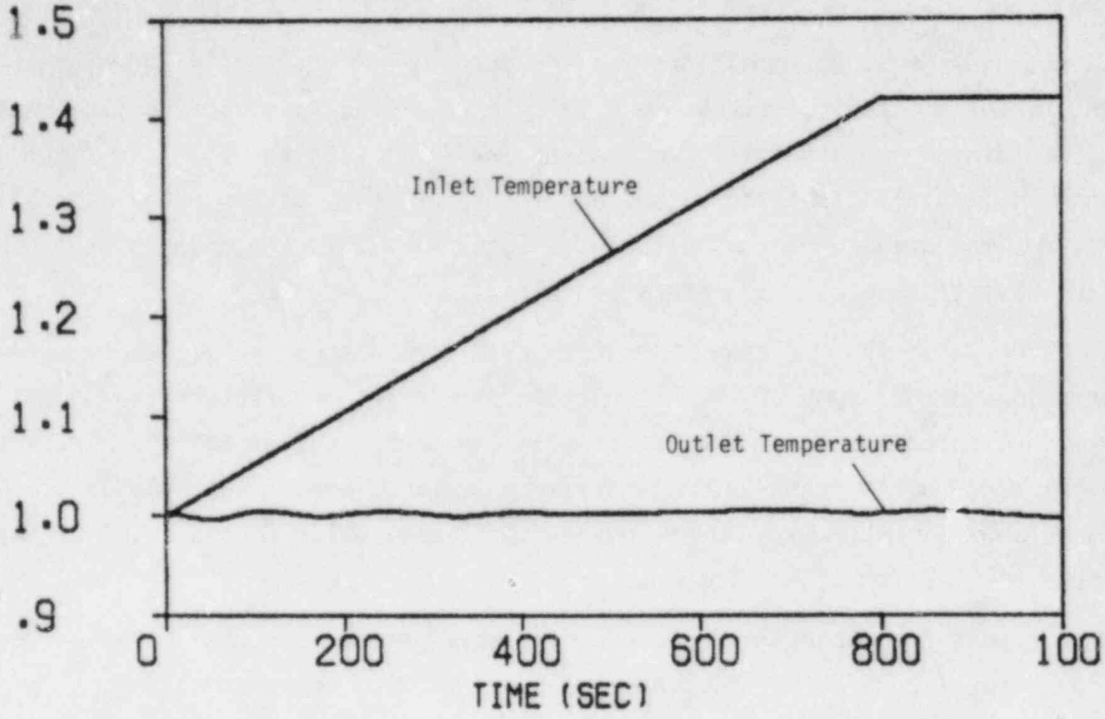

Figure 4.3 Normalized DHX Sodium Temperatures (Ref. case)

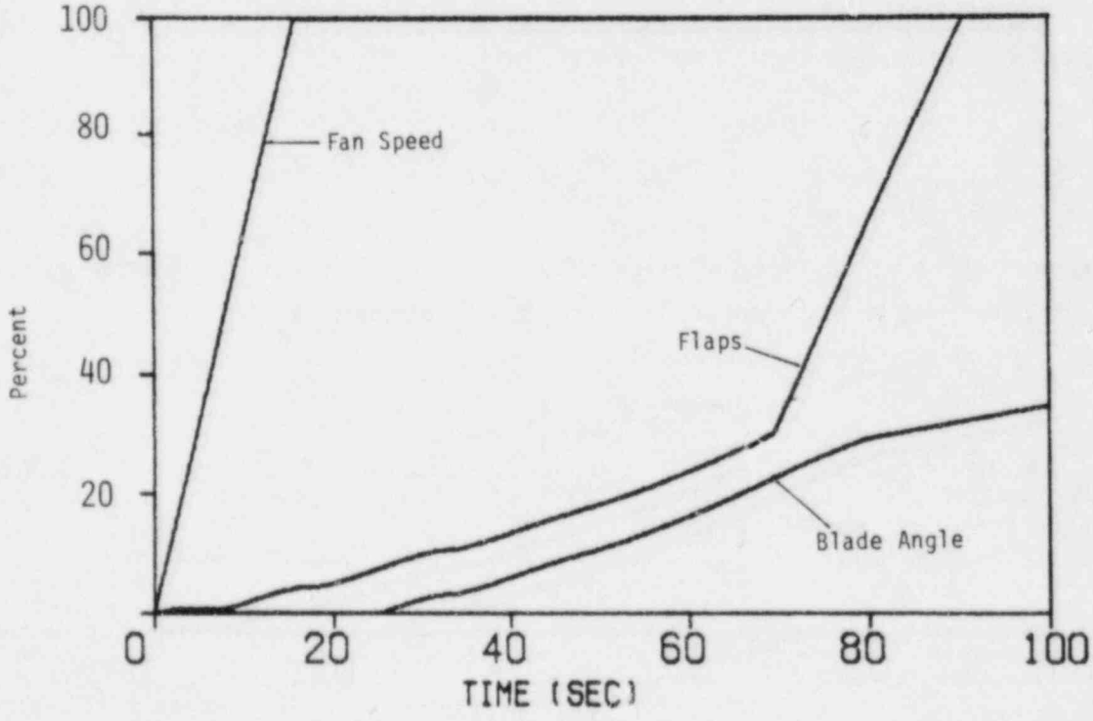

Figure 4.4 Behavior of Air Flow Controller Actuator Elements (Ref. case, normalized)

Because the scram conditions for the DHX are not accurately known at present, several other transients were calculated with varying sodium flow rates (0.5 to 3. x W_{Ref}) and inlet temperature gradients (1.5 to 4.5 K/s). It was found that in all cases the system behaves adequately, although the controller settings may need to be readjusted at a later time when the code is coupled with SSC and/or actual parameters are known.

Figures 4.5 and 4.6 show the responses of the air cooler outlet temperatures to a sudden jump of 25 K/s in the sodium inlet temperature (W_{NA} = 9.5 kg/s). The jump produces oscillations in the sodium outlet and the air side temperature. This transient was chosen in order to verify that the control chain behaves stably even under severe conditions, which is indicated by the damped oscillation of the response.

The post scram controller and the influence of the control valves on the loop hydraulics were tested by solving the following momentum equation:

$$\frac{L}{A}\frac{dW}{dt} = \Delta P_{pump} - \Delta P_{pipe} - \Delta P_{valv}$$

where the time dependent pump behavior after scram was simulated by:

$$\Delta P_{pump} = \Delta P_{pump,Ref}\left(1 - \frac{t}{(t + 5.5)^2}\right)$$

Because the post scram controller uses the reactor power as the demand, the time dependent normalized power after scram was provided by:

$$P = 1 - \frac{t}{t + 5.5}$$

where t is the time after scram.

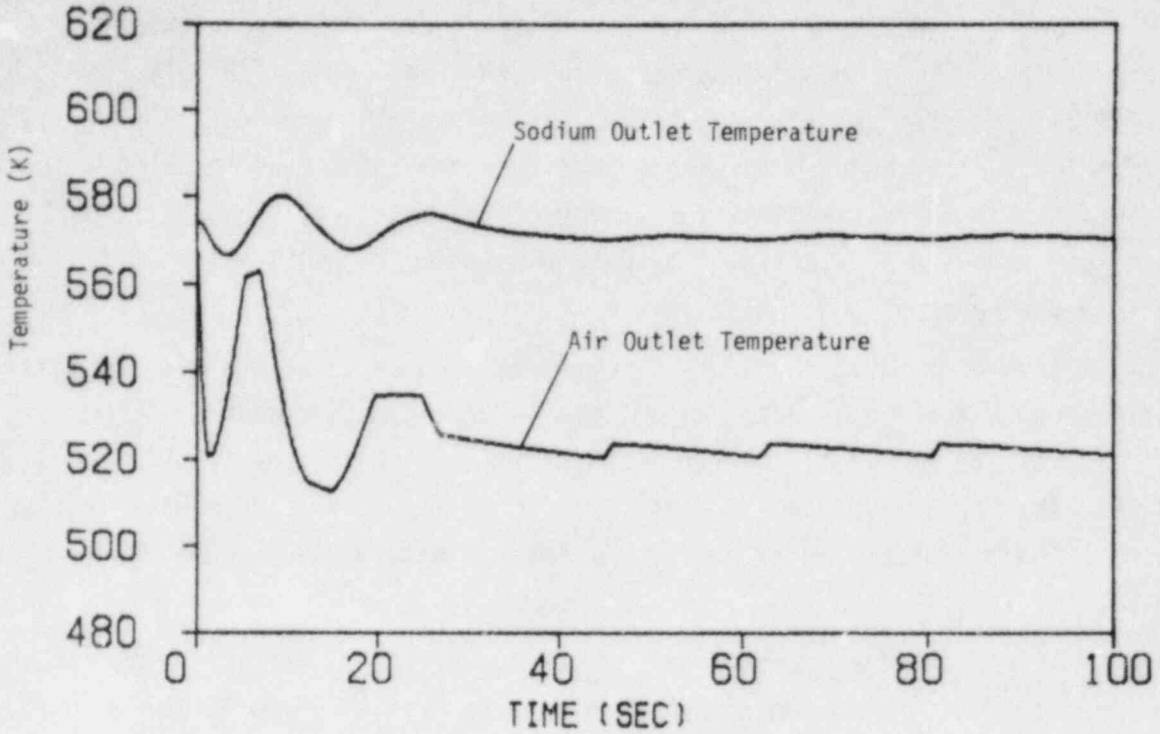

Figure 4.5 DHX - Outlet Temperatures (25 K/s)

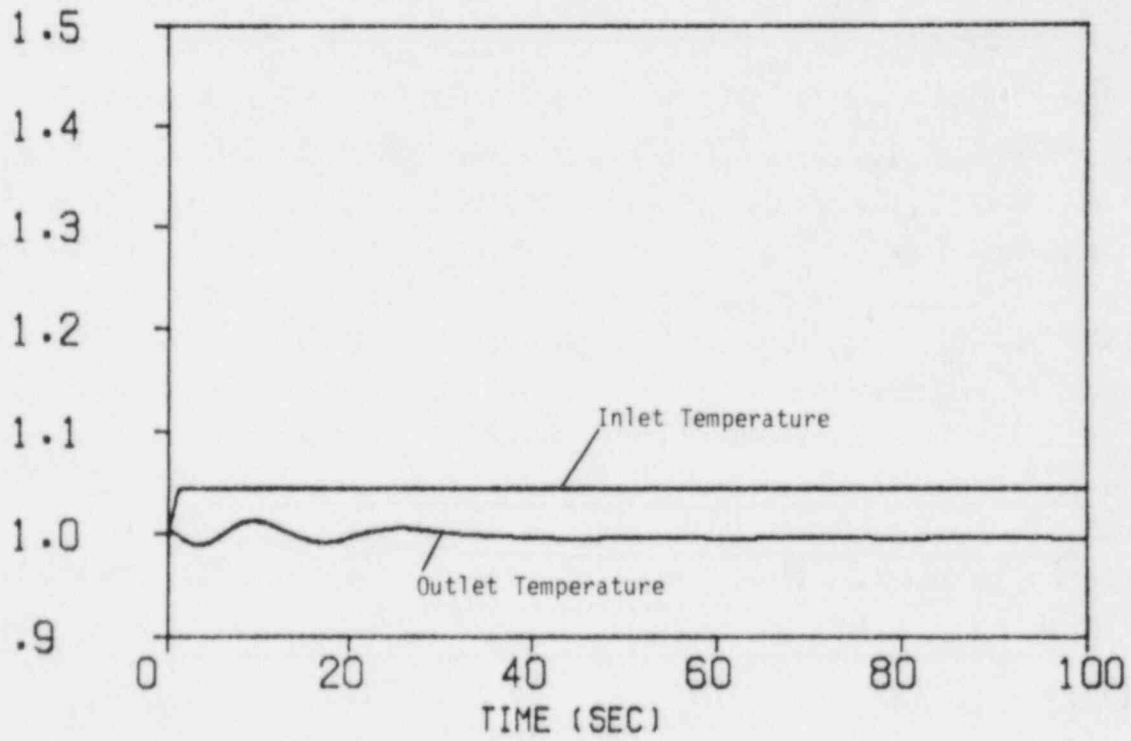

Figure 4.6 Normalized DHX Sodium Temperatures (25 K/s)

Figure 4.7 shows the power and flow rate results obtained without the control valve acting. The power drops much faster and is considerably lower than the flow rate even after 100 seconds. The reason is the unrealistically large L/A value, which was used for the stand-alone model in order to allow a stable solution with large timesteps for test calculations. For $\Delta P_{pump,Ref}$, 0.4E6 N/m^2 was chosen, the starting flow rate was 138 kg/s. Both values are well within the range of the KNK-II reactor.

Figures 4.8 - 4.10 show results obtained from calculations with an active post scram controller. After scram, the valve closes immediately (Fig. 4.9), and forces the flow rate to drop much faster than in the previously described case. The valve continues to close until flow and power are in balance (Fig. 4.8). The corresponding signal of the three point switch is depicted in Fig. 4.10.

After the stand-alone code was successfully tested, attention was focused on checking out the new models when interfaced to SSC. Figures 4.11 - 4.15 show results of the first test run of the post scram controller model in conjunction with the system code SSC. To demonstrate the effect of the controller on the flow rates in the heat removal system and, hence, on the thermal behavior of the reactor, a second run was done with the controllers disabled. These results are also depicted in the figures for comparison purposes.

The test case deals with a KNK-II scram at 0.25 s, followed by pump trips after 0.35 s. The control valves close with a delay of 4 s after scram. Both the primary loop valve and the secondary valve start closing at maximum speed (see Fig. 4.11). The primary valve continues closing until the generated power (which is also used as the demand value for the primary valve controllers) is in equilibrium with the core flow rate. Then the motor valve is switched to a slower speed control. For KNK-II, the secondary control valve is operated initially as follows: 1) valve closes at maximum speed for 8 seconds; 2) valve motion is interrupted for 4 seconds, and 3) subsequent valve closure is done at a slower speed until the secondary flow rate reaches the demand value.

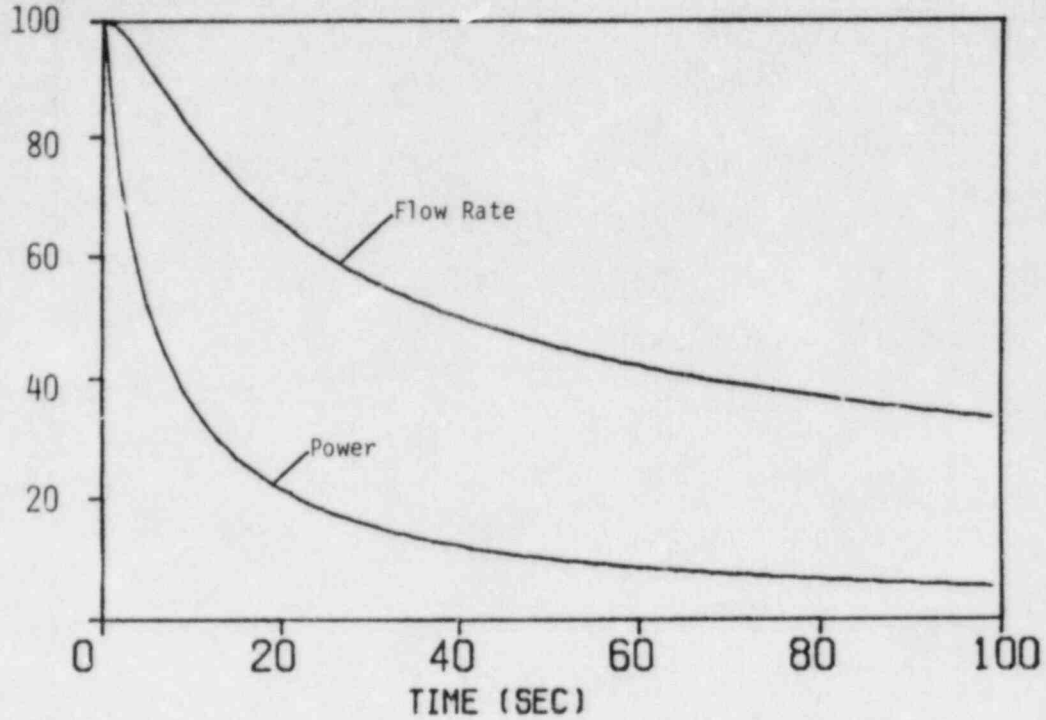

Figure 4.7 Normalized Power and Flow Rate Without Control Valve

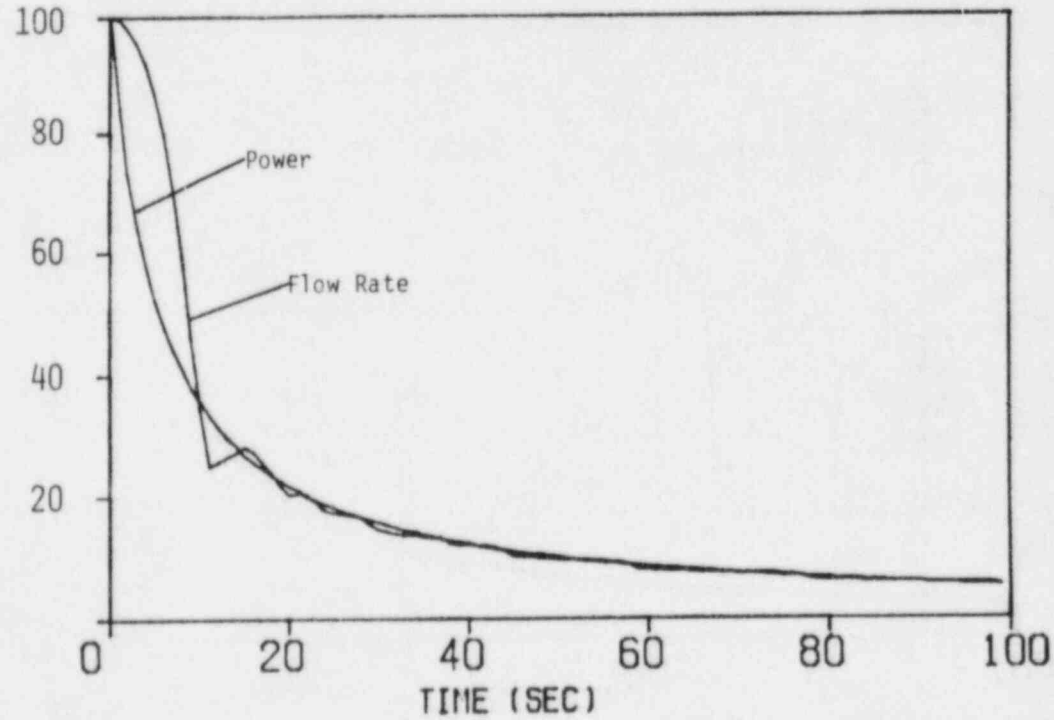

Figure 4.8 Normalized Power and Flow Rate With Active Control Valve

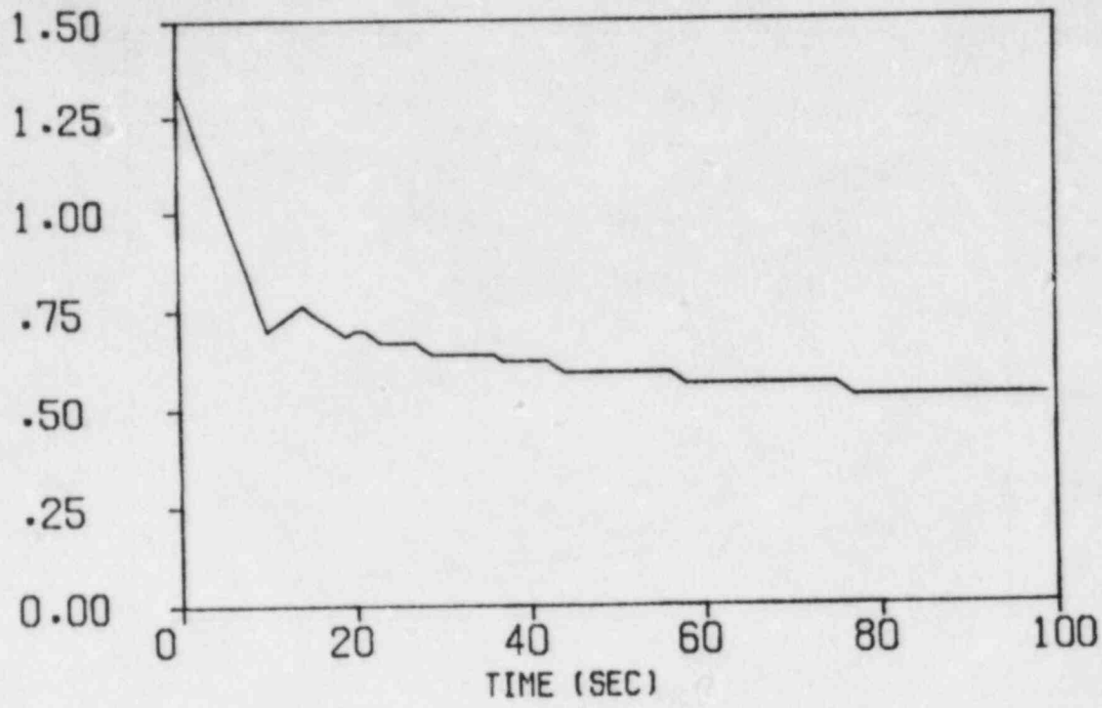

Figure 4.9 Normalized Valve Stem Position

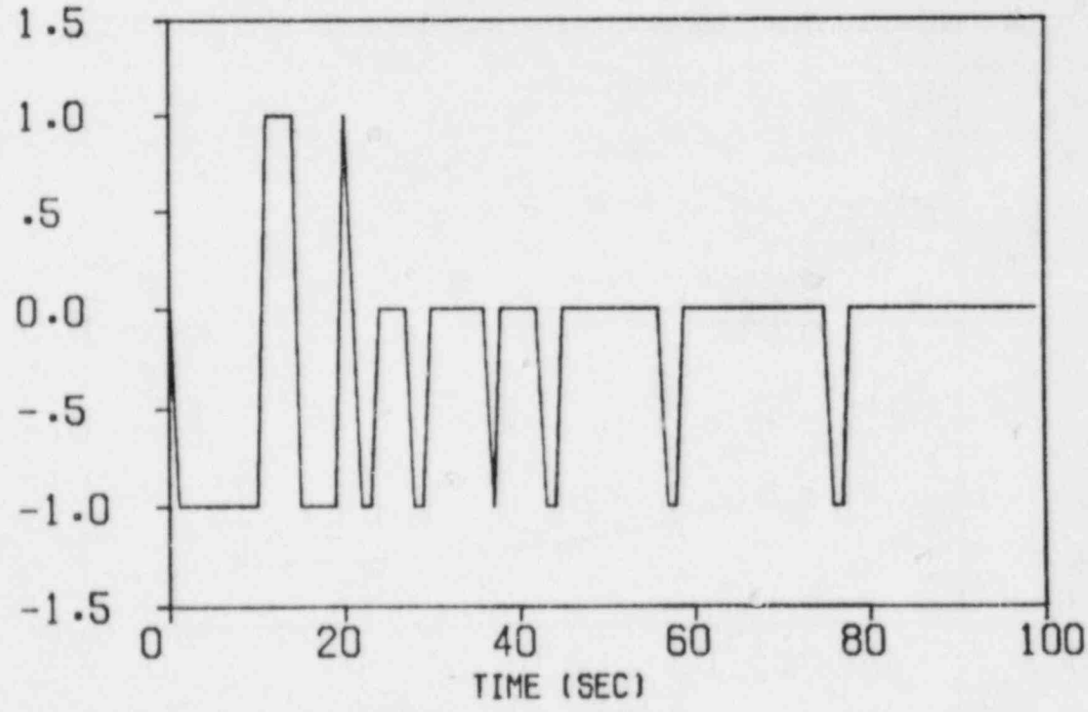

Figure 4.10 Signal of On-Off-On Controller

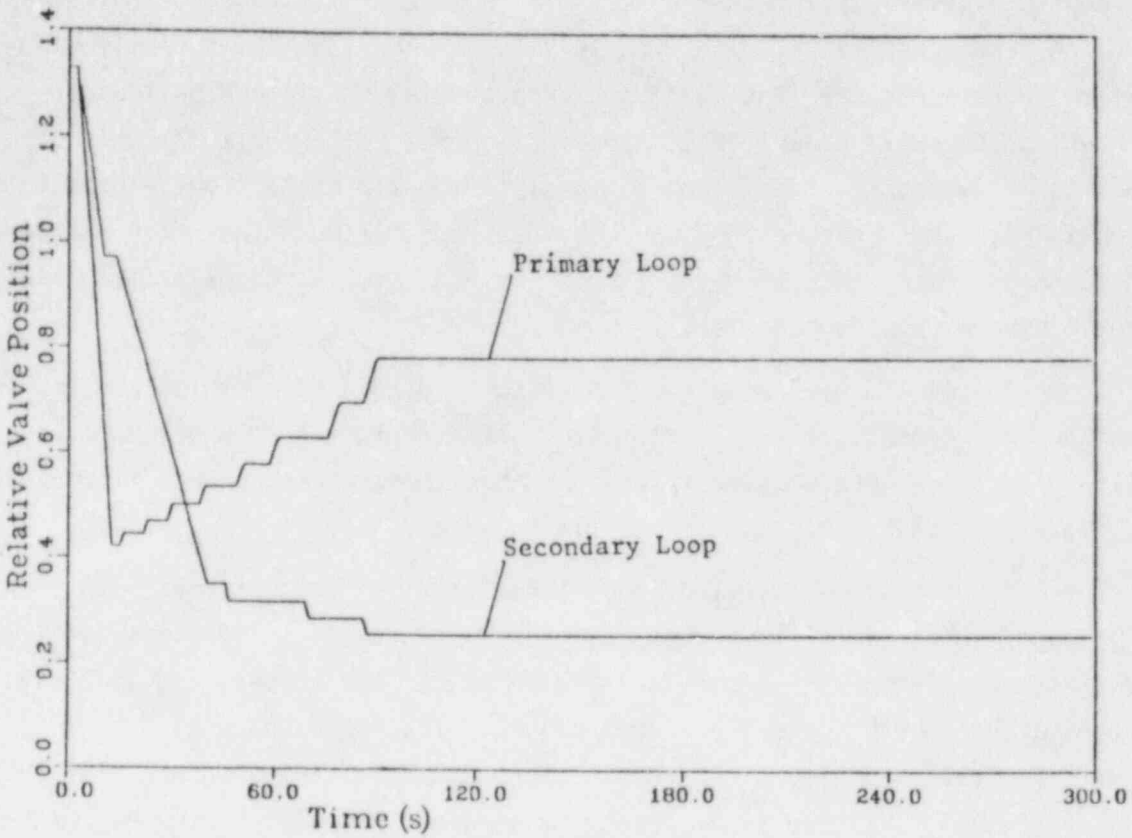

Figure 4.11 Effect of Post Shutdown Control System on Valve Stem Response

In Figures 4.12 and 4.13, the mass flow rates of the primary and secondary loops are shown and compared to the time history of mass flow rates without control valves. For both loops, the flow rate is forced to drop faster to a demand level than in the case without valves. The somewhat surprising behavior of the secondary flow is caused by a special KNK-II design feature, with which the steam generator is bypassed. Here, following scram, the steam generator flow path is closed and a bypass to the air cooler (see Fig. 1.1) is established. The pressure drop through the bypass is much less than through the steam generator and, therefore, the flow rate remains comparatively high for the case without controller.

Figures 4.14 and 4.15 show the temperatures at the core outlet and the reactor outlet, respectively. As expected, the temperature drop due to overcooling is much higher without valves and the temperature recovers slower. The temperature at the reactor outlet nozzle shows a similar trend.

The DHX has also been tested in conjunction with SSC. Figures 4.16 and 4.17 show results of the test run. As already discussed in previous sections, the fan starts immediately after scram occurs. If the temperature limit is reached at the outlet, the flaps open and air flow increases until the sodium outlet temperature drops. The drop is amplified by a slow down of inlet temperature, which is caused by a greatly reduced sodium mass flow rate. After less than 60 s, the air cooler parameters are almost stable, and decay heat removal continues. The slight increase in air flow rate is due to the slowly rising sodium inlet temperature.

5. CONCLUSION

In the previous sections, models have been developed for SSC-L in order to provide certain plant specific design features for post scram transient calculations of the German KNK-II reactor. These models include an Air Dump Heat Exchanger model for controlled heat removal from the intermediate loop and a Post Scram Controller model. Several test calculations show that the models produce reasonable results, both in the stand-alone versions as well as in conjunction with SSC. It is noted that the controller settings need further adjustments. However, because of the lack of experimental data from KNK-II, no validation can be made as yet about the accuracy of the heat exchanger

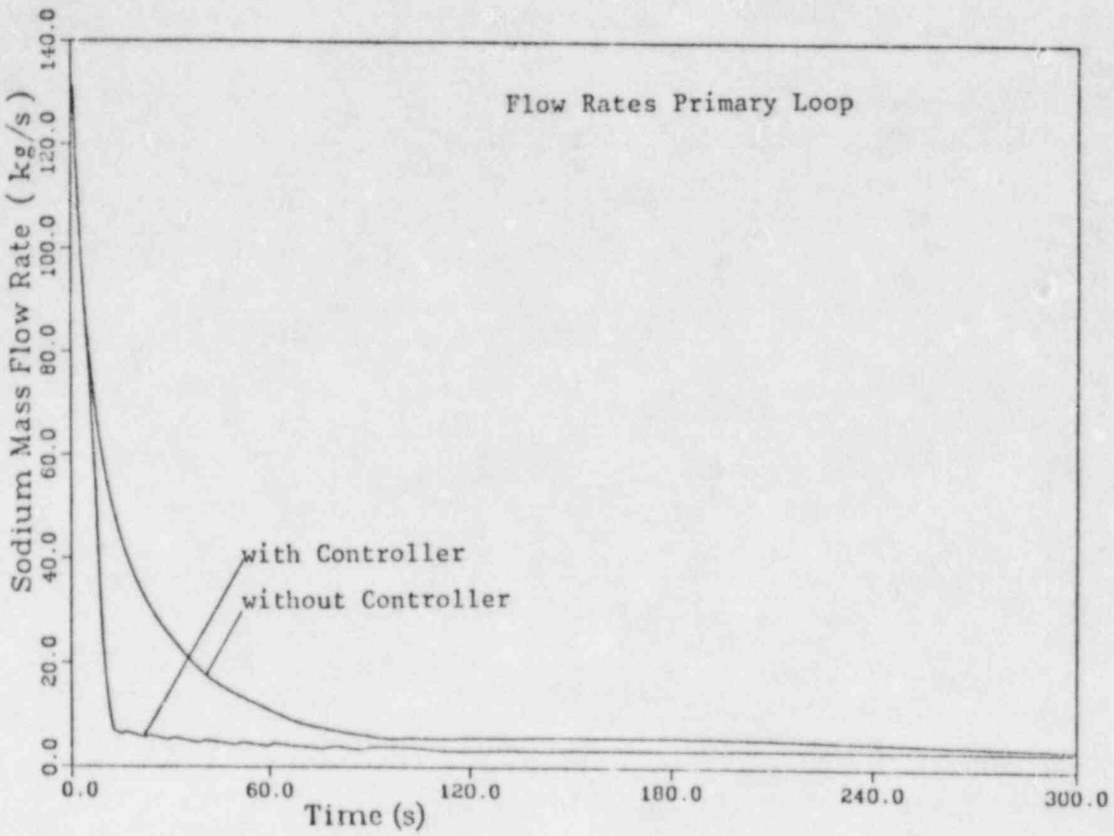

Figure 4.12 Effect of Post Shutdown Control System on Primary Loop Sodium Flow Rate

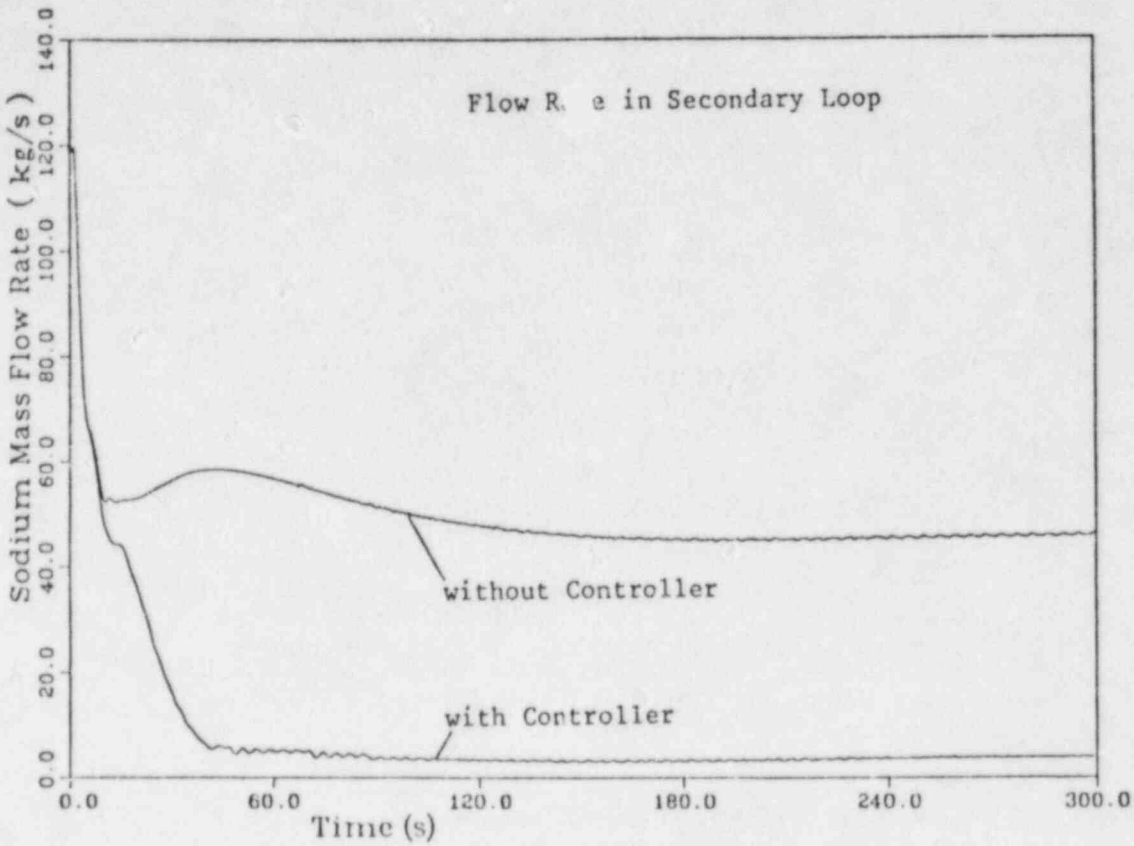

Figure 4.13 Effect of Post Shutdown Control System on Secondary Loop Sodium Flow Rate

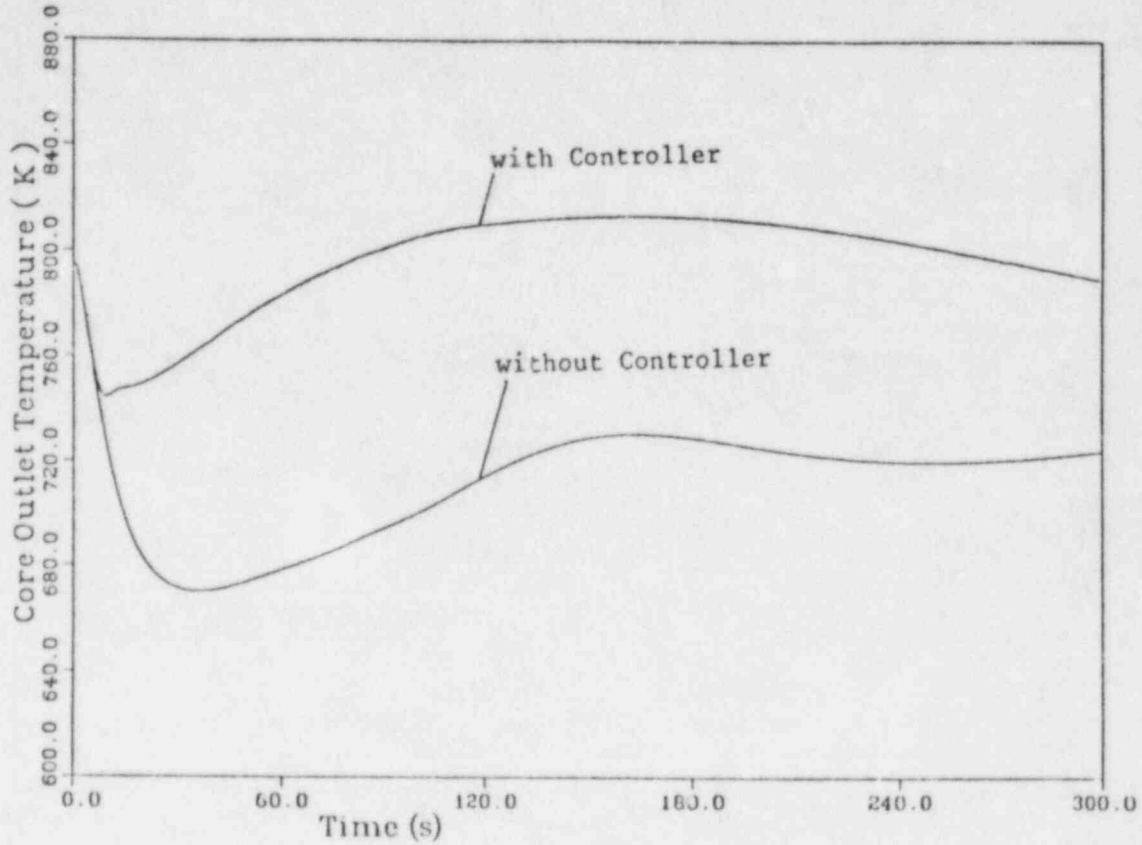

Figure 4.14 Effect of Post Shutdown Control System on Average Core Outlet Temperature

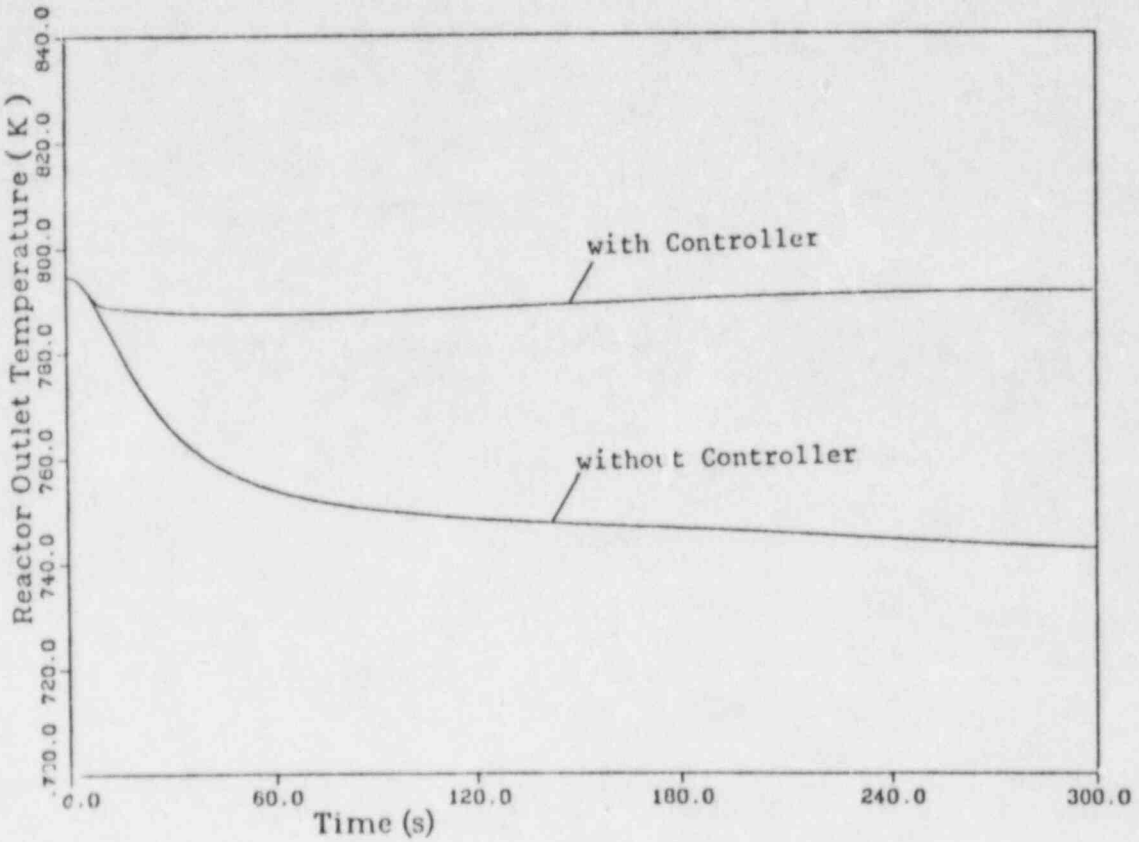

Figure 4.15 Effect of Post Shutdown Control System on Vessel Outlet Temperature

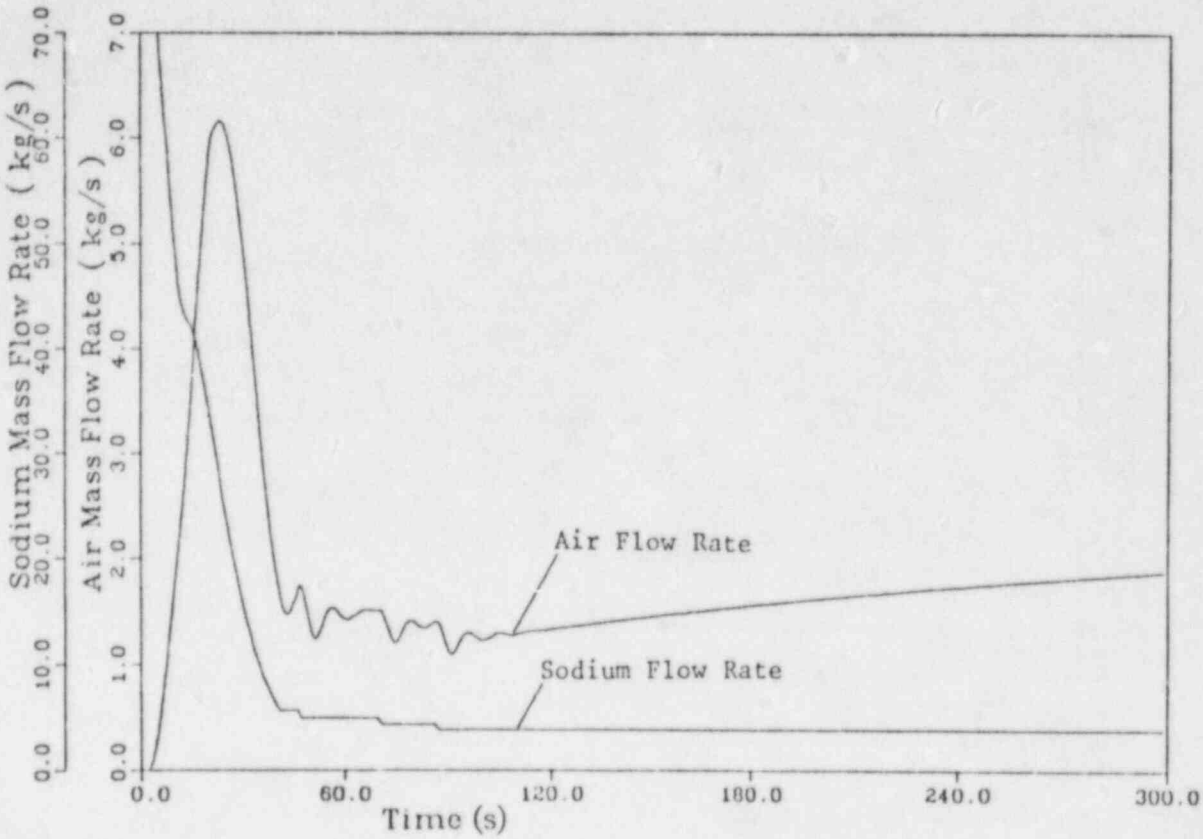

Figure 4.16 Behavior of DHX Flow Rates After Scram

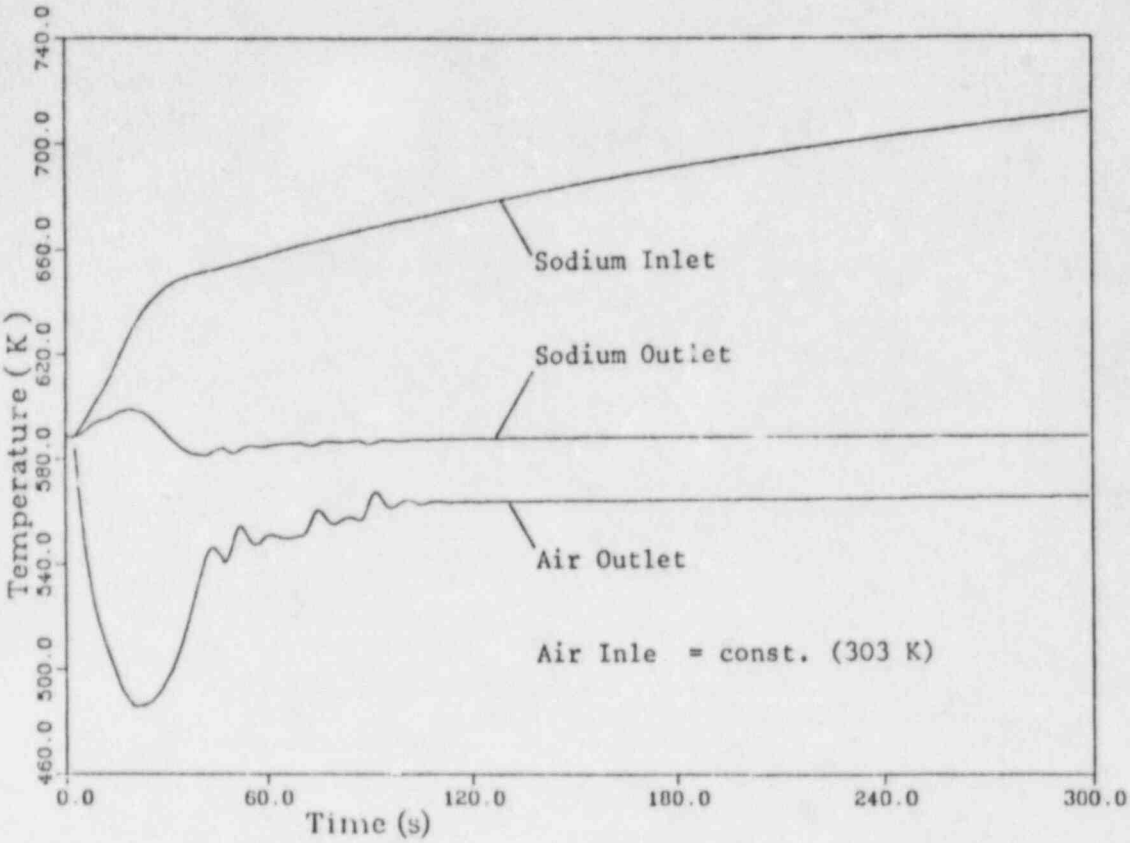

Figure 4.17 Behavior of DHX Temperatures After Scram

model which, for example, uses the assumptions of incompressible air flow and logarithmic mean temperature difference. Therefore, it is recommended that the calculated data be compared as soon as possible against those obtained from KNK-II.

This type of study points up the versatility in the usage of SSC. SSC is a user-oriented, modular computer code that is developed in a very generic fashion. The interfacing of these KNK-II plant-specific models into SSC was accomplished in a straightforward and relatively easy manner.

REFERENCES

1. Atomwirtschaft, No. 2, February 1973.

2. J.G. Guppy, et al., "Super System Code (SSC, Rev. 0), an Advanced Thermo-hydraulic Simulation Code for Transients in LMFBRs," Brookhaven National Laboratory, BNL-NUREG-51650, April 1983.

3. Sicherheitsbericht KNK-II, Band 1-3, INTAT 78.7, 1977.

4. S.S. Kutateladse, et al., "A Concise Encyclopedia of Heat Transfer", Pergamon Press, Oxford, 1966.

5. D.E Briggs and E.H. Young, "Convection Heat Transfer and Pressure Drop of Air Flowing Across Triangular Pitch Banks of Finned Tubes", Chemical Engineering Progress Symposium Series, Vol. 59, No. 41, pp. 1-10, 1963.

6. V.L. Streeter and E.B. Wylie, "Hydraulic Transients", McGraw-Hill, New York,1967.

7. K.B. Cady, "An Air Blast Heat Exchanger System Model", Brookhaven National Laboratory, BNL-NUREG-26237, June 1979.

8. Mohsen Khatib-Rahbar, "Modeling of Plant Protection and Control Systems for SSC", Brookhaven National Laboratory, BNL-NUREG-51241, June 1980.

9. P.J. Roache, "Computational Fluid Dynamics", Hermosa Publishers, 1972.

10. I.K. Madni, "Transient Analysis of Coolant Flow and Heat Transfer in LMFBR Piping Systems", Brookhaven National Laboratory, BNL-NUREG-51179, April 1980.

11. J.W. Hutchinson, "ISA Handbook of Control Valves", Instrument Society of America, Pittsburgh, PA., 1976.

APPENDIX A

Aircooler Model

DRIV4S	Driver routine for initialization and steady-state solution; called from LOOP2S (in SSC): Input: W2NOW, T2NA Output: PDROP
DRIV4T	Driver routine for transient calculation; called from END2T (in SSC): Input: W, T2NA, S2DELT, J8PSR Output: T2NA
INIT4T	Initialization of variables and arrays
HYDR4T (HYDA4T)	Calculation of hydraulics for sodium side (HYDR4T) and air side (HYDA4T); HYDR4T is called by PIPW2T (in SSC): Input: W Output: DPNA
INCNTR	Initialization of controller arrays and variables
EHX4T	Calculation of air cooler temperatures (transient)
EHX4S	Calculation of air cooler temperatures (steady-state)
CNTR4T	Driver routine for air cooler controller
LOGDT	Calculation of log mean temperature difference
FAN4T	Calculation of fan head
FANCON	Calculation of time dependent behavior of fan and flaps
PID	PID-Controller

ADD	Comparator
SENSOR	Sensor behavior
DEAD	Deadband
NORV	Normalization of values
REFV	Finds reference values
INTF	Interface between thermohydraulic and controller
DEMV	Determines demanded value
PRNT4T	Prints results; called from PRNT9T (in SSC)

Post Scram Controller

INCNXR	Initialization of controller arrays and variables; called from CVAL1S (in SSC)
INITXR	Initialization of thermohydraulic variables; called from CVAL1S (in SSC)
CNTRXT	Driver routine for controller; called from DRIV9T (in SSC): Input: J8PSR, S1DELT
VALX	Calculates valve behavior
INTFX	Loads hydraulic values into controller arrays
DPVALX	Calculates valve pressure loss

TRESHX — On-off-on controller

DEMVX — Determines demanded values

CONNXT — Interface between SSC and controller; called from LOOP2S, CVAL1S, CVAL1T, PIPW2T (in SSC);

Input: W, RHOAVG Output: DPNA

PRNTXT — Prints results; called from PRNT9T (in SSC)

☆U.S. GOVERNMENT PRINTING OFFICE 1984 717 032 10008

NRC FORM 335 (11-81)

U.S. NUCLEAR REGULATORY COMMISSION

BIBLIOGRAPHIC DATA SHEET

1. REPORT NUMBER (Assigned by DDC)
NUREG/CR-3910
BNL-NUREG-51806

4. TITLE AND SUBTITLE (Add Volume No., if appropriate)
Dynamic Simulation of the Air-Cooled Decay Heat Removal System of the German KNK-II Experimental Breeder Reactor

2. (Leave blank)

3. RECIPIENT'S ACCESSION NO.

7. AUTHOR(S)
Bernd K. Schubert

5. DATE REPORT COMPLETED
MONTH: June YEAR: 1984

9. PERFORMING ORGANIZATION NAME AND MAILING ADDRESS (Include Zip Code)
Department of Nuclear Energy
Brookhaven National Laboratory
Upton, Long Island, New York 11973

DATE REPORT ISSUED
MONTH YEAR

6. (Leave blank)

8. (Leave blank)

12. SPONSORING ORGANIZATION NAME AND MAILING ADDRESS (Include Zip Code)
Division of Accident Evaluation
Office of Nuclear Regulatory Research
U.S. Nuclear Regulatory Commission
Washington, D.C. 20555

10. PROJECT/TASK/WORK UNIT NO.

11. FIN NO.
A-3015

13. TYPE OF REPORT
Technical Report

PERIOD COVERED (Inclusive dates)

15. SUPPLEMENTARY NOTES

14. (Leave blank)

16. ABSTRACT (200 words or less)

A Dump Heat Exchanger and associated feedback control system models for decay heat removal in the German KNK-II experimental fast breeder reactor are presented. The purpose of the controller is to minimize temperature variations in the circuits and, hence, to prevent thermal shocks in the structures. The basic models for the DHX include the sodium-air thermodynamics and hydraulics, as well as a control system. Valve control models for the primary and intermediate sodium flow regulation during post shutdown conditions are also presented. These models have been interfaced with the SSC-L code. Typical results of sample transients are discussed.

17. KEY WORDS AND DOCUMENT ANALYSIS

17a. DESCRIPTORS

Dynamic Analysis
Control System
LMFBR
Decay Heat Removal
System Analysis Computer Code

17b. IDENTIFIERS/OPEN-ENDED TERMS

18. AVAILABILITY STATEMENT
UNLIMITED

19. SECURITY CLASS (This report)
unclassified

21. NO. OF PAGES

20. SECURITY CLASS (This page)
unclassified

22. PRICE
$

NRC FORM 335 (11-81)